PORTLAND PRESS

Research Article

Human DPSCs fabricate vascularized woven bone tissue: a new tool in bone tissue engineering

Francesca Paino[1]*, Marcella La Noce[1]*, Alessandra Giuliani[2], Alfredo De Rosa[3], Serena Mazzoni[2], Luigi Laino[4], Evzen Amler[5,6], Gianpaolo Papaccio[1], Vincenzo Desiderio[1]§ and Virginia Tirino[1]§

[1]Dipartimento di Medicina Sperimentale, Sezione di Biotecnologie, Istologia Medica e Biologia Molecolare, Università degli Studi della Campania 'L. Vanvitelli', via L. Armanni, 5-80138, Naples, Italy; [2]Dipartimento di Scienze Cliniche Specialistiche e Odontostomatologiche, Università Politecnica delle Marche, Via Tronto 10/a, 60020 Torrette di Ancona, Ancona, Italy; [3]Dipartimento Multidisciplinare Medico-chirurgico, Sezione di Odontostomatologia, Università degli Studi della Campania 'L. Vanvitelli', Via Luigi De Crecchio, 6-80138 Naples, Italy; [4]Dipartimento di Medicina Clinica e Sperimentale, Università degli Studi di Foggia, Plesso di Medicina Viale Luigi Pinto, 1-71122 Foggia, Italy; [5]Department of Biophysics, 2nd Faculty of Medicine, Charles University in Prague, V Úvalu 84, 150 06, Prague 5, Czech Republic; [6]Institute of Experimental Medicine, Academy of Sciences of the Czech Republic, v.v.i., Vídeská 1083, 142 20, Prague 4, Czech Republic

Correspondence: Virginia Tirino (virginia.tirino@unina2.it) and Dr Vincenzo Desiderio (vincenzo.desiderio@unina2.it)

OPEN ACCESS

Human dental pulp stem cells (hDPSCs) are mesenchymal stem cells that have been successfully used in human bone tissue engineering. To establish whether these cells can lead to a bone tissue ready to be grafted, we checked DPSCs for their osteogenic and angiogenic differentiation capabilities with the specific aim of obtaining a new tool for bone transplantation. Therefore, hDPSCs were specifically selected from the stromal–vascular dental pulp fraction, using appropriate markers, and cultured. Growth curves, expression of bone-related markers, calcification and angiogenesis as well as an *in vivo* transplantation assay were performed. We found that hDPSCs proliferate, differentiate into osteoblasts and express high levels of angiogenic genes, such as vascular endothelial growth factor and platelet-derived growth factor A. Human DPSCs, after 40 days of culture, give rise to a 3D structure resembling a woven fibrous bone. These woven bone (WB) samples were analysed using classic histology and synchrotron-based, X-ray phase-contrast microtomography and holotomography. WB showed histological and attractive physical qualities of bone with few areas of mineralization and neovessels. Such WB, when transplanted into rats, was remodelled into vascularized bone tissue. Taken together, our data lead to the assumption that WB samples, fabricated by DPSCs, constitute a noteworthy tool and do not need the use of scaffolds, and therefore they are ready for customized regeneration.

Introduction

Several medical disciplines have focused with increasing interest on the regeneration of organs and tissues damaged by diseases, trauma or ageing, through the use of stem cells, which show the remarkable ability to give rise to a plethora of cell types [1]. The use of autologous and allogeneic stem cells, isolated from various tissues of adults, has fewer ethical problems than the use of embryonic stem cells [2]. One easily accessible source of mesenchymal stem cells is the dental pulp, which is a stromal, fibrous, highly vascularized structure located in the inner part of the tooth [3,4]. Stem cells from human dental pulp stem cells (hDPSCs) express several transcription factors that are involved in the maintenance of self-renewal and pluripotency, such as Sox2 and NANOG [5], and specific mesenchymal stem cell markers, such as CD90 [6]. Under defined culture conditions, hDPSCs differentiate into numerous cell types, including osteogenic, adipogenic, neurogenic and neural crest-derived cells [7–12]. Several studies have shown that hDPSCs can be successfully used in clinical practice as a new therapeutic tool for healing bone defects [13–15].

Important issues have been addressed concerning the clinical use of hDPSCs, including the development of materials that are safe for human use for the isolation and maintenance of cells selected for therapy. Therefore, procedures and good manufacturing practice (GMP) protocols are needed for the culture of the stem cells for clinical use. In this context, it seems that GMP-approved human serum (HS) may be of interest for use in cell manipulation. Another important point arises from the capability of these stem cells to fabricate, already *in vitro*, samples of bone tissue.

A major task in this research was to find advanced techniques that could verify and quantify the mineralization process and the neovascularization of the proposed bone substitutes, at the early stages of bone formation. In this context, third-generation synchrotron sources, producing brilliant photon beams with high spatial coherence properties, have been demonstrated to be suitable for these studies [16,17] by the application of phase-sensitive, X-ray imaging methods.

Therefore, the aim of the present study was to challenge the differentiation potentials of DPSCs, assessing their capability of directly producing a transplantable bone tissue and evaluating their histological and physical properties *in vitro*, as well as their behaviour after *in vivo* transplantation, for direct use in human bone tissue engineering.

Materials and methods
Human dental pulp extraction and cell culture

Human dental pulps were extracted from teeth of healthy adults (aged 21–38 years). Before the extraction, each individual ($n = 40$) was checked for systemic and oral infections or diseases. Only patients undergoing a third molar or supernumerary tooth extraction were interviewed and enlisted. All participants signed the Ethical Committee (Second University Internal Ethical Committee) consent form before being enrolled. Every participant was pretreated for a week with professional dental hygiene. The dental crown was covered with 0.3% chlorhexidine gel (Forhans) for 2 min before the extraction. Dental pulp was obtained with a dentinal excavator or a Gracey curette. The pulp was delicately removed and immersed for 1 h at 37°C in a digestive solution composed of 3 mg/ml of type I collagenase and 4 mg/ml of dispase in PBS containing 40 mg/ml of gentamicin. Once digested, the solution was filtered through 70 μm Falcon strainers (Becton & Dickinson). Cells were cultured in basal growth medium consisting of Dulbecco's modified Eagle's medium (DMEM) with 100 units/ml of penicillin, 100 mg/ml of streptomycin and 200 mM L-glutamine (all from Gibco), supplemented with 10% heat-inactivated AB-HS (Invitrogen). Cells were maintained in a humidified atmosphere under 5% CO_2 at 37°C and the media were changed twice a week.

Growth analysis and soft-agar assay

Cells were plated at a density of 50000 cells/well in 6-well plates and at a density of 100000 cells in T25 flasks; growth curves were performed at 24, 48 and 72 h, and 7, 14 and 21 days of culture. The cells were harvested and re-suspended in PBS. An aliquot of cell suspension was diluted with 0.4% Trypan Blue (Sigma-Aldrich), pipetted on to a haemocytometer and counted under a microscope. The number of viable cells for each experimental condition was counted and represented on a linear graph. The doubling time (DT) was determined from the growth curves or by using the formula:

$$DT = (t - t_0) \log_2 / (\log N - \log N_0)$$

where t and t_0 were the times at which the cells were counted, and N and N_0 were the cell numbers at times t and t_0, respectively.

In order to assay the possible tumorigenic potential, cells were plated in soft agar at a density of 500 or 1000 cells/well in 24-well plates in triplicate. The Colo 38 melanoma cell line was used as the positive control cell line. For the base layer, 0.8% soft agar was used. For the top layer, the agar stock solution was diluted with culture medium to obtain a solution of 0.3% agar in DMEM. Cells were successively plated and incubated for 21 days at 37°C in a humidified atmosphere of 5% CO_2 in air. Colonies were stained with 150 μl/well of Nitroblue Tetrazolium at the concentration of 0.5 mg/ml in PBS, and counted using an inverted microscope (Nikon TS 100).

FACS analysis

Flow cytometry analyses were performed on hDPSCs at first passage of culture. Cells were incubated with FITC-conjugated anti-CD90, PerCP-Cy5.5-conjugated anti-CD105, APC-Cy7-conjugated anti-CD45 (all purchased from BD Pharmingen), and PE-conjugated anti-CD34 (Miltenyi Biotech) for phenotypic characterization, and FITC-conjugated anti-bone sialo-protein (BSP) (Biorbyt), anti-CFS-conjugated anti-osteopontin (OPN) (R&D Systems) and PerCP-Cy 5.5-conjugated anti-NANOG (BD Pharmingen) for evaluation of osteogenic differentiation and

Table 1. Primer sets used for RT-PCR

Gene	Forward primer (5′-3′)	Reverse primer (5′-3′)	Ta
GAPDH	GGAGTCAACGGATTTGGTCG	CTTCCCGTTCTCAGCCTTGA	57°C
RUNX2	CACTCACTACCACACCTACC	TTCCATCAGCGTCAACACC	52°C
bALP	TCAAACCGAGATACAAGCAC	GGCCAGACCAAAGATAGAGT	58°C
BGLAP	CTCACACTCCTCGCCCTATTG	CTTGGACACAAAGGCTGCAC	58°C
OPN	GCCGAGGTGATAGTGTGGTT	TGAGGTGATGTCCTCGTCTG	58°C
BSP	GGGCAGTAGTGACTCATCCG	TTCTCAGCCTCAGAGTCTTCA	58°C
OSTERIX	TCCTCCCTGCTTGAGGAGGA	AGTCCCGCAGAGGGCTAGAG	60°C
CXCR4	CCTATGCAAGGCAGTCCATGT	GGTAGCGGTCCAGACTGATGA	57°C
INTβ1	CATCTGCGAGTGTGGTGTCT	GGGGTAATTTGTCCCGACTT	57°C
VEGF	TGACAGGGAAGAGGAGGAGA	CGTCTGACCTGGGGGTAGAGA	60°C
PDGFA	ACACGAGCAGTGTCAAGTGC	GGCTCATCCTCACCTCACAT	60°C
COL1A1	GAGGCTCTGAAGGTCCCCA	CACCAGCAATACCAGGAGCA	60°C
DSPP	TTGTTGAAAACTCTGTGGCTGTGC	GGCATCGTTGAAAATGCGGAGGAA	60°C

mesenchymal stemness. As negative controls, cells were stained with an isotype control antibody. After incubation with the antibody, cells were re-suspended in PBS and analysed using an FACS ARIA III or BD Accuri C6 (BD Biosciences). Human DPSCs were then sorted for CD34- and CD90-positive markers. The purity of sorting was approximately 90%.

For intracellular staining of osteocalcin (OC), OPN and NANOG, cells were processed using a Fix & Perm Kit (Invitrogen) following the manufacturer's guidelines. All data were analysed using FCS express version 3 (De Novo Software).

RNA isolation and semiquantitative PCR

Total RNA was extracted from hDPSCs after 7, 14, 21 and 40 days of culture, using an Ambion kit (Invitrogen, Life Technologies Italia) following the manufacturer's instructions. RNA was treated with DNase (Promega) to exclude DNA contamination and stored at $-80°C$. Complementary DNA synthesis was carried out from total RNA (1 μg) using VILO SuperScript (Invitrogen). PCR analyses were carried out using a Bioer LifePro Thermal Cycler (Life Technologies Italia) in which samples underwent a 2 min denaturing step at 94°C, followed by 35 cycles at 94°C for 30 s, 52–60°C for 60 s, 72°C for 30 s, and a final extension step at 72°C for 4 min. Each PCR reaction was performed in a total volume of 12.5 μl containing 10 mM Tris buffer, pH 8, 0.2 mM of each dNTP, 1.5 mM MgCl$_2$ and 0.2 μM of each primer, 1 unit of Taq DNA polymerase and 1 μl of each cDNA. PCR was carried out using primer sequences and annealing temperatures listed in Table 1. The amplification products were separated on a 2% agarose gel in Tris/acetate EDTA (TAE) buffer. The transcript amount of each gene was normalized to glyceraldehyde 3-phosphate dehydrogenase (GAPDH). Relative expression was calculated using ImageJ software (NIH).

Alizarin Red staining

After 28 days of culture, osteogenic phenotype was evaluated using Alizarin Red staining to visualize calcium-rich deposits produced by the cells. The samples were washed twice in PBS, fixed with 4% paraformaldehyde (PFA) in PBS for 30 min at 4°C, and stained with 2% Alizarin Red solution, pH 4.2 (Sigma Aldrich) for 20 min at room temperature. Stained cells were extensively washed with deionized water to remove any non-specific precipitation. Micrographs were taken using a microscope Eclipse TE2000-S (Nikon) and a Nikon camera.

Immunofluorescence analysis

After 21 days of culture, hDPSCs seeded in 24-well plates were fixed with 4% PFA in PBS for 20 min at room temperature. After washing in PBS, samples were permeabilized with 0.1% Triton X-100 for 5 min and blocked with 1% BSA in PBS. Incubation with primary anti-OC antibody (sc-30044, Santa Cruz) was performed overnight at 4°C. Primary antibody was revealed using an FITC-conjugated, anti-rabbit immunoglobulin G, secondary antibody. Nuclei were stained with Hoechst stain.

Micrographs were taken with a microscope EVOS FL Cell Imaging System (Life Technologies).

ELISA

To evaluate vascular endothelial growth factor (VEGF) levels produced by hDPSCs and released in the medium, a VEGF ELISA was performed using a VEGF Human ELISA kit (Thermo Fisher) according to the manufacturer's protocol. The media were collected at 7, 14 and 21 days. VEGF concentrations were read versus a standard curve at 450 nm using a spectrophotometer (DAS Plate Reader). The experiments were performed in triplicate.

Production of a woven bone tissue in culture

After 40 days of culture in standard medium, DPSCs give rise to samples of woven bone (WB), i.e. fibrous bone with a low level of mineralization. The appearance of these bone samples was scattered within each flask. They grow and build up into rounded 3D structures. The final thickness of the obtained tissue was related to the medium level height, and it was possible to obtain samples up to 15 mm in length. The area of the newly formed tissue could easily reach 1 cm^2. WB samples were fixed in 4% PFA and paraffin. Paraffin-embedded WB sections were rehydrated with xylene, a decreasing scale of alcohols (100%, 95% and 75%) and distilled water, and were then stained with Alizarin Red S.

In vivo transplantation

WB samples, each sized 4×4 mm, were subcutaneously transplanted into the dorsal surface of 10-week-old athymic nude rats (Charles River Laboratories International, Inc.), with the purpose of assaying the capability of WB to give rise to well-vascularized and mature bone tissue. A total of 10 animals were used in this study. Similar samples of the same size were also used to test their ability to regenerate mandibular vertical defects. For this, mandibular defects were created in 10 athymic nude rats, according to previously described procedures [3,18,19]. Briefly, all athymic nude rats underwent general anaesthesia with isoflurane. A first incision of the left mandible was performed by a blade in order to expose the mandibular body. The latter underwent electrocautery to dissect the pterygomasseteric sling. Then, after measuring a 5×5 mm square of mandible defect with a pen, bone tissue was removed using a 1 mm high-speed cutting burr set at 3000 rev./min. WB samples were placed in the defect using resorbable sutures. After transplantation, athymic nude rats received analgesia using buprenorphine at the concentration of 0.1 mg/kg for up to 3 days and trimethoprim/sulfamethoxazole for up to 7 days to prevent infection. Athymic nude rats were monitored every 3 days and, 30 days after transplantation, they were sacrificed and the tissues collected for histology and immunofluorescence assay. Tissue samples were fixed in 4% PFA and decalcified with buffered 10% EDTA, pH 7.4. Paraffin-embedded tissue sections were rehydrated with xylene, a decreasing scale of alcohols (100%, 95%, and 75%) and distilled water, and were then stained with haematoxylin and eosin (H&E), Mallory's Trichrome stain or Alizarin Red S. For immunofluorescence, tissue sections were treated with 5% milk for 1 h, and incubated overnight at 4°C with anti-human class I HLA antibody (Abcam) to assess the human origin of the tissue and anti-human CD34, OC and type I collagen (COLIA1; all from Abcam). Secondary antibodies were goat anti-rabbit FITC and TRITC (Abcam). The nuclei were stained with Hoechst stain, and the tissue samples were observed under the microscope (EVOS, Life Technologies). Isotypes and non-probed tissue sections were used as controls. The transplantation experiments were performed in triplicate. All animal experiments were approved by our internal animal ethics committee of the University of Campania 'L. Vanvitelli' of Naples.

Synchrotron X-ray phase-contrast microtomography and holotomography

Human DPSC cultures, 40 days from the start of culture, were dehydrated in a graded ethanol series (70%, 75%, 80%, 85%, 90%, 95% and 100%) with three changes at each concentration and 10 min between steps, and dried under a hood overnight before phase-contrast microtomography (phc-microCT) and holotomography (HT).

For phc-microCT analysis, a white beam without any filter was used with a sample-to-detector distance of 150 mm (corresponding to a single-distance phase-contrast set-up) and voxel size of $2.1 \times 2.1 \times 2.1 \ \mu m^3$ for all the samples ($n = 3$). The exposure time was set to approximately 1 s per projection, with a total of 1800 radiographic images for all the samples. The reconstruction of the tomographic slices was performed using a phase-sensitive approach. The phase contrast, in the edge-enhancement regimen, differs from conventional X-ray imaging because the resulting images are not solely based on attenuation contrast. The effect of the X-ray beam going through the sample is described by the refractive index, $n(r) = 1 - \delta(r) + i\beta(r)$, where $\delta(r)$ is the refractive index decrement and $\beta(r)$ the attenuation index. As $\delta(r)$ is much larger than the imaginary part when studying weakly absorbing substances such as our DPSC cultures, the phase approach provides greater sensitivity than the absorption approach, which is normally used for fully mineralized tissues. $\delta(r)$ is actually proportional to the mean electron density, which in turn is almost proportional to the mass density. The method used for quantitative volumetric reconstructions of the refractive index n is based on a two-step approach: first, the phase projections are determined in the form of radon projections

(phase retrieval) and then the object function, i.e. the refractive index decrement $\delta(r)$, is reconstructed by applying a conventional filtered-back projection (FBP) algorithm.

Typically, the phase retrieval implies the reconstruction of two different real-value 3D distributions, $\delta(r)$ and $\beta(r)$; such reconstruction generally requires acquisition of at least two different 2D projections at each angle of view. However, in some cases, it can be shown by assuming that the distributions of the real and imaginary parts of the refractive index are proportional to each other, i.e. $\delta(r) = \varepsilon \cdot \beta(r)$, where the proportionality constant ε does not depend on the spatial coordinates. This assumption is possible only for special classes of objects, such as *pure-phase* (i.e. very weakly absorbing) objects, or *homogeneous* objects, such as objects consisting predominantly of a single material (possibly with a spatially varying density). This last case is represented by the present hDPSC cultures in which, at the early stages of bone formation, there is a slow variation of the complex amplitude ('monomorphous' specimen). In this situation, a single projection per each view angle is sufficient for reconstruction of the 3D distribution of the complex refractive index [20].

In this study, a phase-retrieval algorithm based on the transport of intensity equation (TIE) [21,22] was applied to the acquired datasets, with parameters tuned to edge-enhancement reduction and balance-noise minimization. Then, the FBP algorithm was used to reconstruct the slices. The XTRACT software (CSIRO Mathematical and Information Sciences) was applied for both the TIE-based phase retrieval and the reconstruction of X-ray phase-contrast slices.

Volume rendering is a 3D visualization method by which data volumes are rendered directly, without the need for decomposition into geometric primitives. A Quad-Core Processor 2.01 GHz PC with 8 GB RAM and the commercial software VG Studio MAX 1.2 (Volume Graphics) were used to generate 3D images and visualize the phase distribution in 3D. Optimal image quality settings were obtained using the scatter HQ algorithm with an oversampling factor of 5.0 and activated colour rendering. X-ray contrast differences within samples translate into different peaks in the grey-level scale, corresponding to the different phases. The volume of each phase was obtained by multiplying the volume of a voxel by the number of voxels underlying the peak associated with the relevant phase. The mixture modelling algorithm (Plugin of ImageJ software, version 3) was implemented to threshold the histograms. Thresholded slices were used to automatically separate the different phases.

For the evaluation of the regenerated bone in DPSC cultures, the following quantitative descriptors were used: the bone volume:total volume ratio (BV/TV – expressed as a percentage), the bone surface:bone volume ratio (BS/BV – expressed in mm^{-1}) and the newly formed bone thickness (BTh – expressed in micrometres).

The morphometric analysis was also performed using VG Studio MAX 1.2.

A fourth hDPSC sample, also at 40 days from culture, and a Bio-Oss control were also submitted to HT. HT was performed with an ID19 Beamline (ESRF) using a beam energy of 20 keV. The radiographs were recorded with a cooled CCD camera (ESRF FReLoN) with a 14-bit dynamic range, 2048×2048 pixels and pixel size of 678 nm; 1500 projections were recorded over $180°$ sample rotation at detector–sample distances of 7, 29, 59 and 119 mm.

The HT approach differs from the phc-microCT method based on a single distance previously described. Here the acquisition took advantage of four different 2D projections at each view angle, allowing observation in the 3D reconstructions of the presence of new vessels and extracellular matrix (ECM), which, because of their low attenuation coefficient, are transparent in conventional attenuation-based tomographic reconstructions.

Solely for HT, we used a method of phase retrieval that has recently been used in experiments and described [23]. For this assay, for a better evaluation of the WB sample features, they were analysed constantly comparing their physical properties with those of human healthy mandibles and an acellular matrix, namely a commercial Bio-Oss (Geistlich AG Wolhusen).

Statistical analysis

Values are shown as the means±S.E.M.s of measurements of at least three independently performed experiments to avoid possible variation of cell cultures. Student's *t*-test was used, and $P < 0.05$ was considered to be statistically significant. Quantitative morphometric phc-microCT data are shown as means±S.D.s.

Results
Characterization and sorting of hDPSCs

At the first culture passage, cells were characterized by evaluating the expression of CD90, CD105, CD34 and CD45 using cytometric analysis. Cells were all positive for the mesenchymal markers CD90 and CD105, and negative for CD45. The expression of CD34 was approximately 20% (Figure 1A). This characterization is of paramount importance because only these cells constitute the stromal–vascular fraction of the dental pulp and are capable of giving rise to differentiation towards bone and vessels. Human DPSCs were sorted for CD34- and CD90-positive markers.
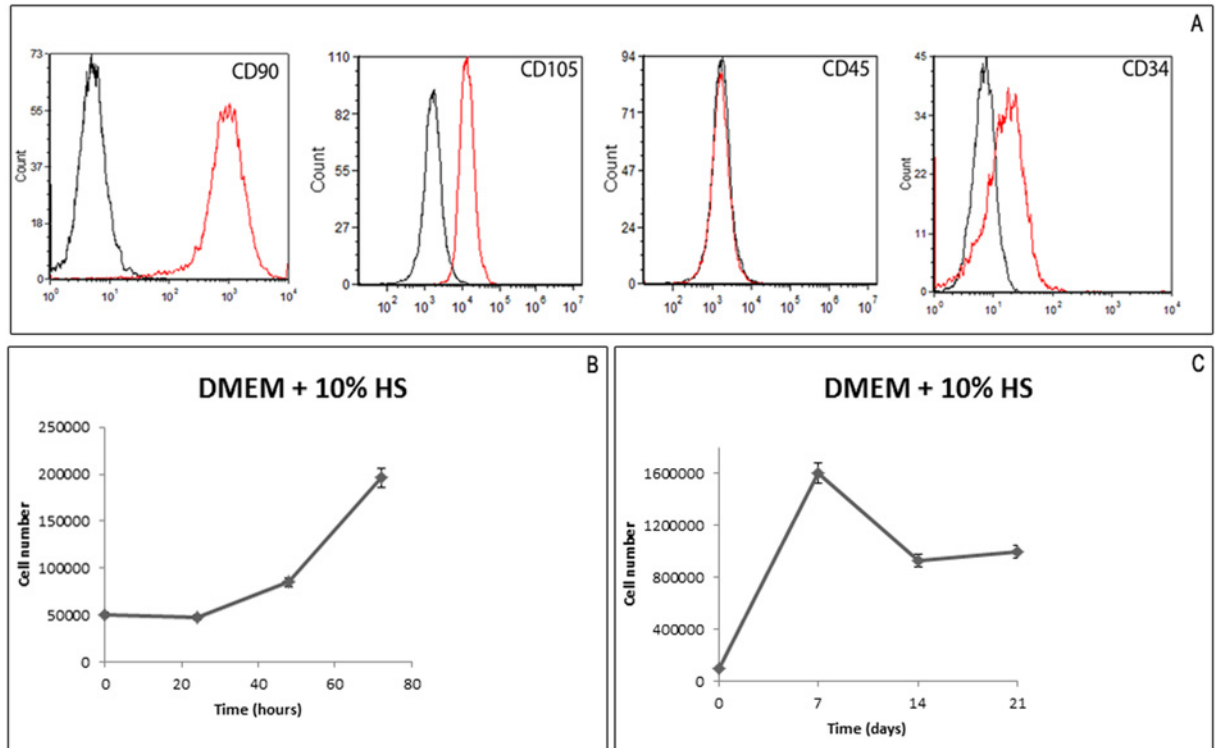
Figure 1. Characterization and growth of DPSCs

(**A**) Characterization of DPSCs at the first passage of culture: cytometric analysis of CD90, CD105, CD45 and CD34 markers in DPSCs. Histograms represent the number of cells (*y*-axis) and fluorescence intensity (*x*-axis) relative to unstained control cells (black histogram), and cells marked with specific antibodies against surface proteins (red histogram). (**B**) Growth curve of DPSCs: the average DT is 49 ± 2 h. (**C**) Growth performance was studied for up to 21 days.

Evaluation of cell proliferation and colony formation

Cell proliferation was evaluated at 24, 48 and 72 h (Figure 1B), and 7, 14 and 21 days (Figure 1C) of culture. Human DPSCs were found to actively proliferate, mainly during the first week (Figure 1B), with an average DT of 49 ± 2 h. Anchorage-independent growth is the ability of transformed cells to grow independently of a solid surface, and is a hallmark of carcinogenesis. The assay of soft-agar colony formation is a well-established method for characterizing this capability *in vitro* and is considered to be one of the most stringent tests for malignant transformation in cells. Human DPSCs did not form colonies in soft agar.

Analysis of stemness and osteogenic differentiation

In order to evaluate hDPSC stemness and osteogenic differentiation, a flow cytometric assay at different days of culture for CD90, CD34, NANOG, BSP and OPN was performed (Figure 2A). Human DPSCs showed positivity (>98%) for the mesenchymal marker CD90. Levels of the stromal–vascular antigen CD34 decreased up to day 21. Expression of the stemness marker NANOG also decreased. The expression of osteogenic markers showed that BSP peaked at day 7 and then decreased; conversely, the expression of OPN increased significantly at 14 days.

Taken together, these results show that DPSCs produced a significant amount of proteins, such as BSP and OPN, involved in osteogenic differentiation. Further investigations on osteogenic differentiation were also performed using a semiquantitative PCR for COLIA1, RUNX2, bone alkaline phosphatase (bALP), BSP, OPN, OC, Osterix, at 7, 14 and 21 days of culture (Figure 2B). RUNX2 expression, the master transcription factor of osteogenic differentiation, significantly increased. The expression of OPN mRNA did not change over time as well as the levels of bALP.

BSP, OC and Osterix, a transcriptional factor activated in late osteogenic differentiation, were increased at 7 days of culture. COLIA1 increased at 14 days of culture and remained similar at 21 days. At 14 and 21 days, the expression of OC was unchanged. At 14 and 21 days, BSP continued to decrease. Conversely, Osterix mRNA levels remained
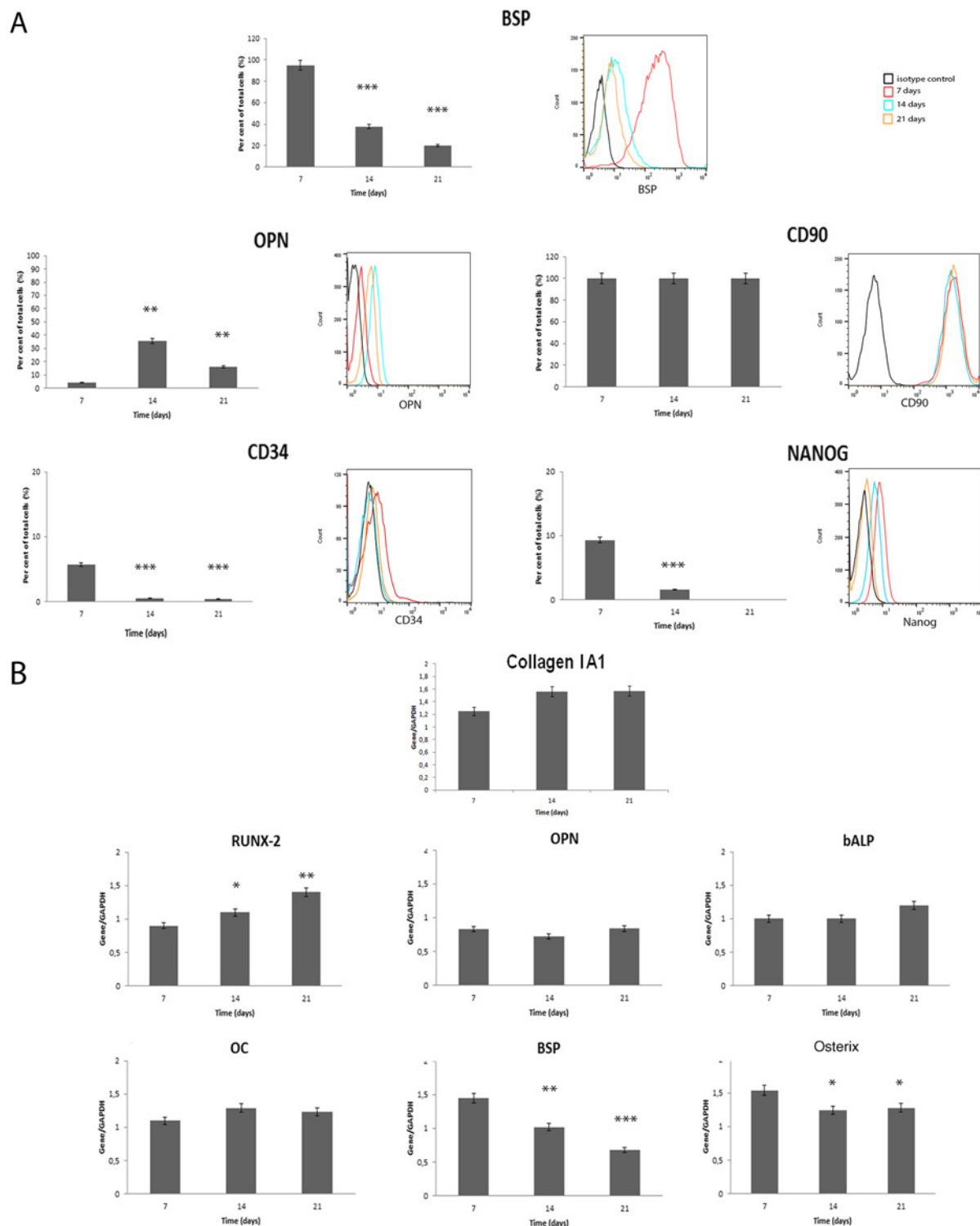
Figure 2. Cytometric analysis and gene expression in DPSCs

(**A**) Cytometric analysis and (**B**) gene expression for osteogenic markers, and stemness markers (L–N) in DPSCs. $^{*}P < 0.001$, $^{**}P < 0.0005$, $^{***}P < 0.0001$ compared with the cell line at day 7.
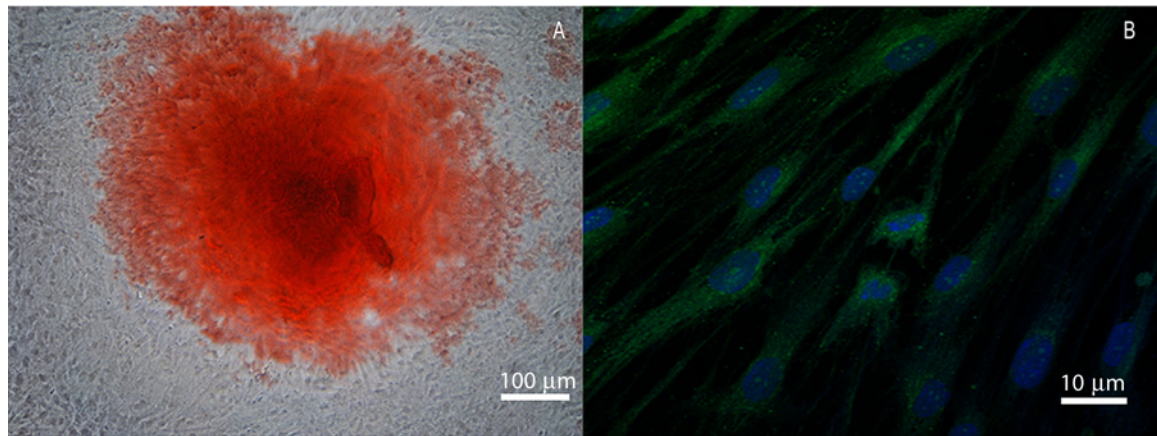
Figure 3. Alizarin Red analysis of DPSCs
(**A**) Representative images showing Alizarin Red staining. Scale bar = 100 μm. (**B**) Immunofluorescence analysis for OC. Scale bar = 10 μm.

high at both 14 and 21 days. In addition, dentin sialophosphoprotein (DSPP) mRNA expression was negative (data not shown), reinforcing the idea that the hDPSCs were devoted to the bone lineage.

Evaluation of mineralization and intracellular localization of OC

For better characterization of bone differentiation, Alizarin Red S staining and OC distribution were evaluated. Alizarin Red staining showed the formation of large nodules distributed in the flasks (Figure 3A). Immunoreactivity for OC was found to be noticeable at 21 days of culture (Figure 3B). Moreover, we observed that OC was located in the peripheral region of the cytoplasm.

Homing, chemotaxis and evaluation of angiogenesis

In order to evaluate a possible effect in homing and chemotaxis, we assessed the expression of integrin β_1 (ITGβ_1) and chemokine receptor type 4 (CXCR4). ITGβ_1 mRNA peaked only at 7 days of culture (Figure 4A). The expression of CXCR4 was induced at 14 days of culture, and drastically decreased in all the samples at 21 days (Figure 4B).

The expression of VEGF and platelet-derived growth factor A (PDGF-A) mRNAs in hDPSCs was also evaluated after numerous days of culture by semiquantitative PCR (Figure 4C and D). The expression of VEGF mRNA was significantly promoted, a trend retained throughout all the experimental conditions (Figure 4C). In contrast, VEGF release was initially similar at both 7 and 14 days of culture, but then it significantly increased at 21 days ($P < 0.001$) (see Supplementary Figure S2). The expression of the *PDGFA* gene was high at 7 and 21 days of culture, whereas, at 14 days of culture, expression was decreased (Figure 4D). Human DPSCs were negative for PDGF-B mRNA (data not shown).

In vivo grafting of WB samples

At the end of the culture period, DPSCs formed WB, made of fibrous bone (Figure 5A), as demonstrated by Alizarin Red S staining (see Supplementary Figure S1A). WB samples, transplanted subcutaneously into the dorsal hypodermal layer of rats, formed a highly vascularized bone tissue (Figure 5B and C). After 30 days of transplantation, H&E staining revealed that xenografted WB was consistently remodelled into bone tissue (Figure 5B), in which osteocytes, periosteum and vessels were detectable, as indicated using Mallory's Trichrome staining (Figure 5C).

This bone was intensely positive to class I HLA (Figure 5D–F), which confirmed the human origin of the tissue. It is interesting that the detection of human neoangiogenesis was assessed by human CD34, which resulted in being strongly positive on vessels (Figure 5G–I). In addition, this tissue was positive to Alizarin Red S (see Supplementary Figure S1B) and expressed OC and COL1A1 (see Supplementary Figure S1C and D).

When transplanted in mandibular bone defects, after 30 days, WB samples formed a mature bone of lamellar type (Figure 6A and B). Histological evaluation revealed the presence of osteocytes included in lacunae and lamellae (Figure 6A). Moreover, structures resembling haversian canals were also detectable (Figure 6B).
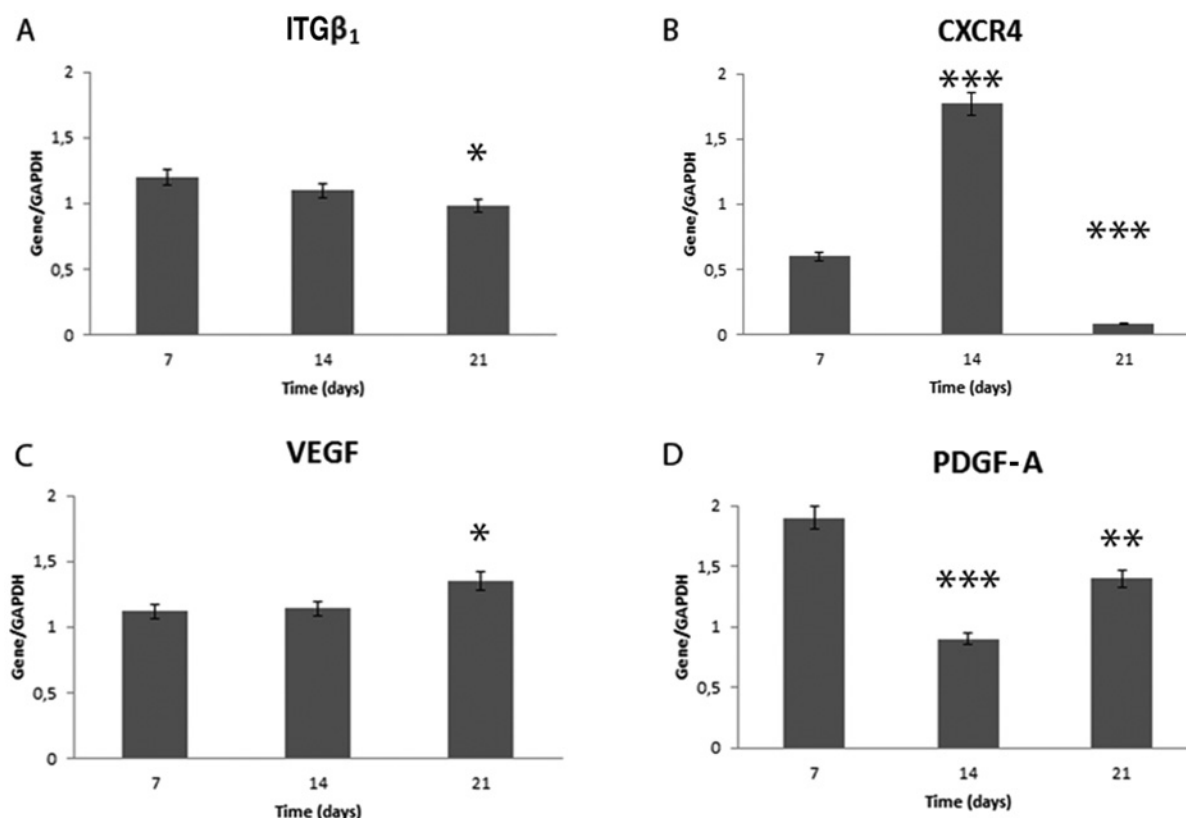
Figure 4. Reverse transcription PCR for genes involved in chemotaxis, cell adhesion and angiogenesis

In (**A**) and (**B**) are shown, respectively, expression of ITGβ_1 and CXCR4 mRNA in DPSCs. In (**C**) and (**D**) VEGF and PDGF-A mRNA levels are shown in DPSCs. All results were normalized to GAPDH expression. $^*P < 0.001$, $^{**}P < 0.0005$, $^{***}P < 0.0001$ compared with the cell line at day 7.

phc-microCT analysis of WB

The osteogenic potential of WB fabricated after *in vitro* hDPSC culture, as shown above in the present study, was validated by the quantitative data extracted from the 3D phc-microCT analysis. MicroCT could easily distinguish in 3D the newly formed bone phase from the hDPSC culture, producing images in which two different phases with different refractive indices were evident. The WB matrix and the newly formed mineralized clusters were coloured using 3D display software to make them more easily recognizable (Figure 7). The woven structure is shown in white, whereas the newly formed mineralized bone (produced by the cells grown in the construct) is depicted in magenta (Figure 7C).

Due to the experimental phase-contrast set-up and the TIE algorithm implemented for the data analysis (Figure 7A and B), the grey levels – here referred to an unsigned 8-bit scale – are proportional to the refractive index decrement $\delta(r)$, which in turn is almost proportional to the mass density ρ of the different phases found inside the sample.

The amount of the newly formed mineralized portion (magenta phase in Figure 7C) was calculated and the data obtained were expressed as BV/TV (%), i.e. the volume ratio of the newly formed bone structure (BV) to the total construct volume (TV), as BS/BV (mm^{-1}), i.e. the newly formed bone specific surface, and as the mean BTh ($\pm \mu$m), i.e. the thickness of the bone clusters. These mean parameters are reported in the bottom insert of Figure 7, together with their S.D.s.

HT analysis of WB

For HT analysis, the volume of interest (VOI) considered was $895 \times 1016 \times 1376 \, \mu$m^3, divided into a stack of 8 (172 μm thick) voxel datasets in the vertical (z) direction. The voxel datasets (32-bit-float volumes per sample) were converted into the respective signed 8-bit datasets (grey scale from -128 to $+127$), and the distribution of grey values analysed using the software package VG Studio MAX 1.2. In both the samples, WB and the Bio-Oss used as a control, the
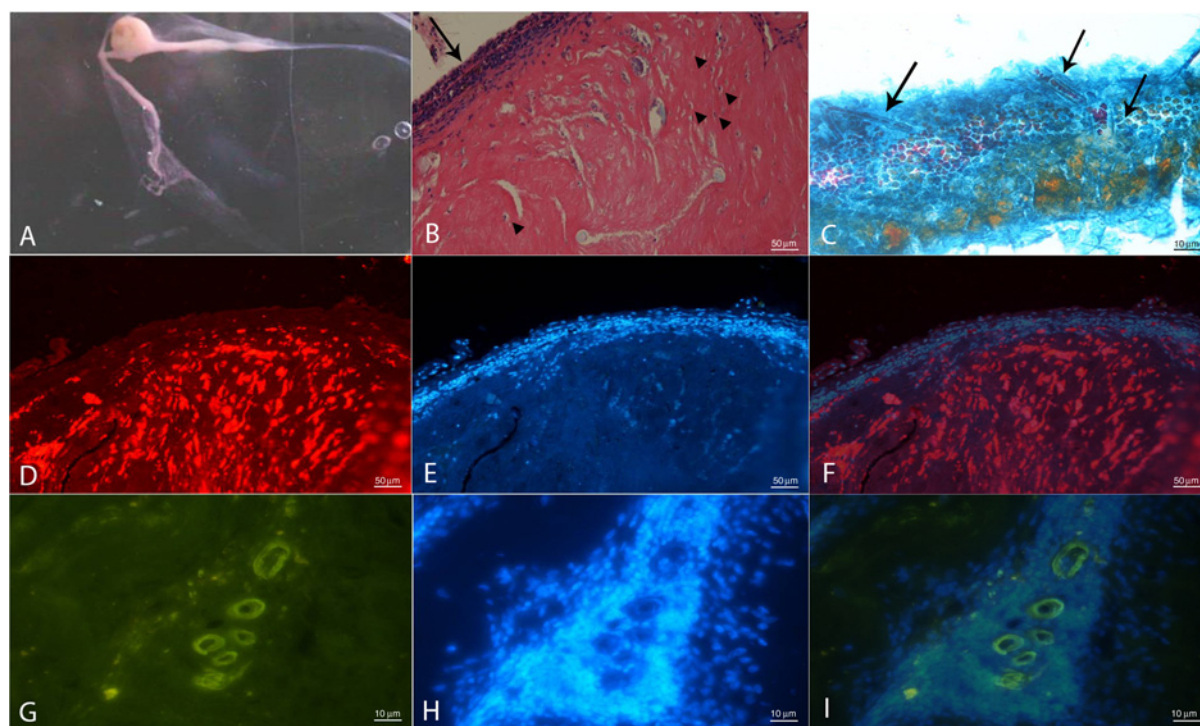
Figure 5. *In vivo* subcutaneous transplantation of WB into rats
(**A**) In the flask, a single WB sample measuring 1×1 cm is shown; (**B**) H&E stain showing *in vivo* bone tissue formation, in which osteocytes (arrowheads) and periosteum (arrows) can be observed; (**C**) Mallory's Trichrome stain showing *in vivo* vessel neoformation (arrows); (**D**) class I HLA positivity on *in vivo* bone tissue sample; (**E**) Hoechst stain of nuclei; (**F**) class I HLA positivity merge on *in vivo* bone tissue sample. (**G**) CD34 positivity on *in vivo* bone tissue sample; (**H**) Hoechst stain of nuclei; (**I**) CD34 positivity merges on *in vivo* bone tissue sample. Scale bars (C, G, H, I) = 10 and (B, D, E, F) = 50 μm.
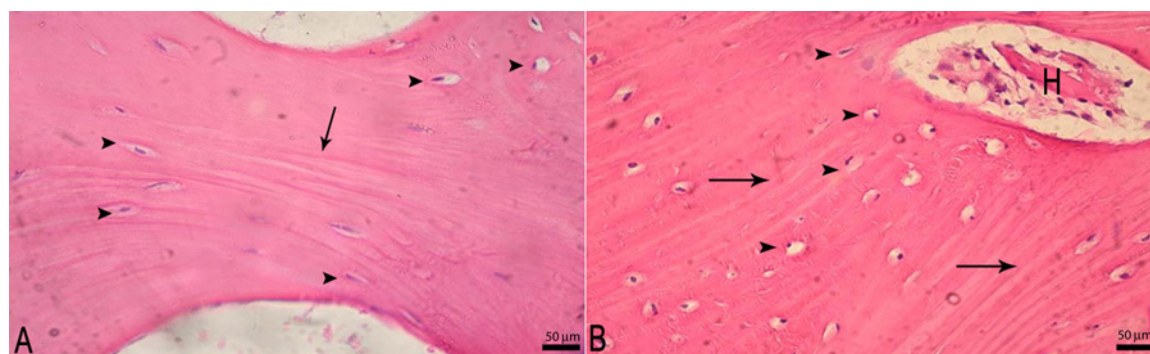

Figure 6. *In vivo* transplantation of WB in a mandibular vertical defect
(**A**) H&E stain showing *in vivo* lamellar bone tissue formation with osteocytes (arrowheads) and lamellae (arrow); and (**B**) haversian canal formation (H) surrounded by lamellae and osteocytes in their lacunae (arrowheads). Scale bars = 50 μm.

histograms could be formally divided into three sectors: the first (furthest left), with an x-value < -50, represented a fully mineralized phase (i.e. high bone mineral density); the second (middle) corresponded to not fully mineralized bone (i.e. a low bone mineral density); the third (furthest right), with an x-value > 0, represented unmineralized phases (air, cells, extracellular matrix, vessels, etc.). The histograms are shown in Figure 8(A) in which it is also reported that the histogram referred to a healthy mandibular biopsy.

Taking into account that the grey levels are proportional to $\delta(r)$, the refractive index decrement, it was found that the profile of the Bio-Oss was similar to that of the human healthy mandibular control biopsy; in fact, both
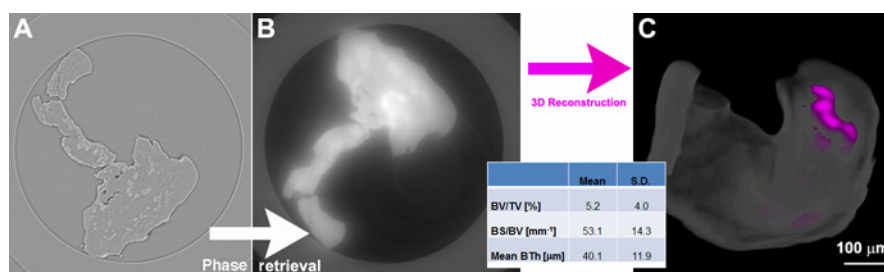
Figure 7. Phase-contrast microCT analysis of WB

(**A**) Two-dimensional slice without phase-retrieval processing: the edge-enhancement signal prevents a reliable discrimination and quantification of the two phases (WB and newly mineralized bone). (**B**) The same 2D slice as in (A) but after phase-retrieval processing; and (**C**) 3D reconstruction of the 2D slices previously processed by phase retrieval: the woven structure is shown in translucent white, whereas the newly formed mineralized bone is depicted in magenta; (bottom inset) morphometric analysis of the 3D volumes.

samples presented coexisting areas of mineralized and unmineralized tissue, although the Bio-Oss presented a larger distribution of mineralized bone, with areas of higher mineralization with respect to mature human bone and areas with lower densities with respect to human bone under remodelling.

It is interesting that the profile of the WB sample was different with respect to both the Bio-Oss and the human healthy mandibular control samples: it presented a huge peak corresponding to not-fully mineralized bone, with lower density with respect to human bone under remodelling. In any case, it must be shown (Figure 8A, inset top left) that a few spots of fully mineralized bone were already formed.

In Figure 8(B), two representative subvolumes of Bio-Oss are shown: one, referring to the histological analysis, was used as a reference (Figure 8B, panel a); the other is the 3D HT reconstruction and respective data analysis (Figure 8B, panels b–d). Two phases are represented in the HT images: bone, independently of its degree of mineralization, and ECM (Figure 8B, panels b–d). One or more phases can be made translucent or even 'cancelled' in order to improve observation of the spatial distribution of the other phases. In Figure 8(B, panel b), the unmineralized phases, apart from that representing unmineralized ECM (visualized in yellow), have been virtually deleted for better visualization of the bone (in shades of grey) and ECM. HT 3D reconstructions (Figure 8B, panels b–d) demonstrated that Bio-Oss is mainly made of strongly mineralized bone. In Figure 8(B, panel c), the ECM has been virtually deleted for better observation of bone morphology, which presents inhomogeneous mineralization. In Figure 8(B, panel d), only densities compatible with the ECM have been visualized: there is a clear evidence of cell absence consequent on decellularization.

This analysis was repeated for the WB sample (Figure 8C): it is evident that here the matrix is WB with few areas of mineralization (Figure 8C, panels a–c). Moreover, there is 3D evidence of newly formed vessels (red arrowheads in Figure 8C, panel d); in fact density signals compatible with neovessels were found in several areas of the investigated WB sample.

Discussion

In the present study, HS was used during expansion and differentiation of hDPSCs *in vitro*, using GMP-approved HS. Freshly isolated hDPSCs were found to be positive for common mesenchymal stem cell markers. Later, hDPSCs were characterized during culture, and the differences in cell proliferation, stemness and osteogenic differentiation assessed.

Significant cell growth was detectable during the culture period. The expression of the CD90 marker remained unchanged throughout all the experimental conditions, indicating that these cells maintained the mesenchymal lineage, whereas the expression of NANOG decreased with time, implying that differentiation of the cells occurred. Human DPSC differentiation leads to a rather early osteoblast formation and ECM deposition; in fact, we noticed an increased expression of markers involved in ECM formation, namely BSP, COLIA1 and OPN, within 14 days, as well as clear Alizarin Red staining of ECM nodules. Moreover, OC expression, at the time, showed that OC mRNA had already been expressed at 7 days of culture, whereas OC protein, detected by immunofluorescence, was slightly distributed along the peripheral region of the cytoplasm. The latter is due to the fact that OC, as far as it is released in the ECM, binds calcium, forming mineralized nodules that are stained with Alizarin Red [24].
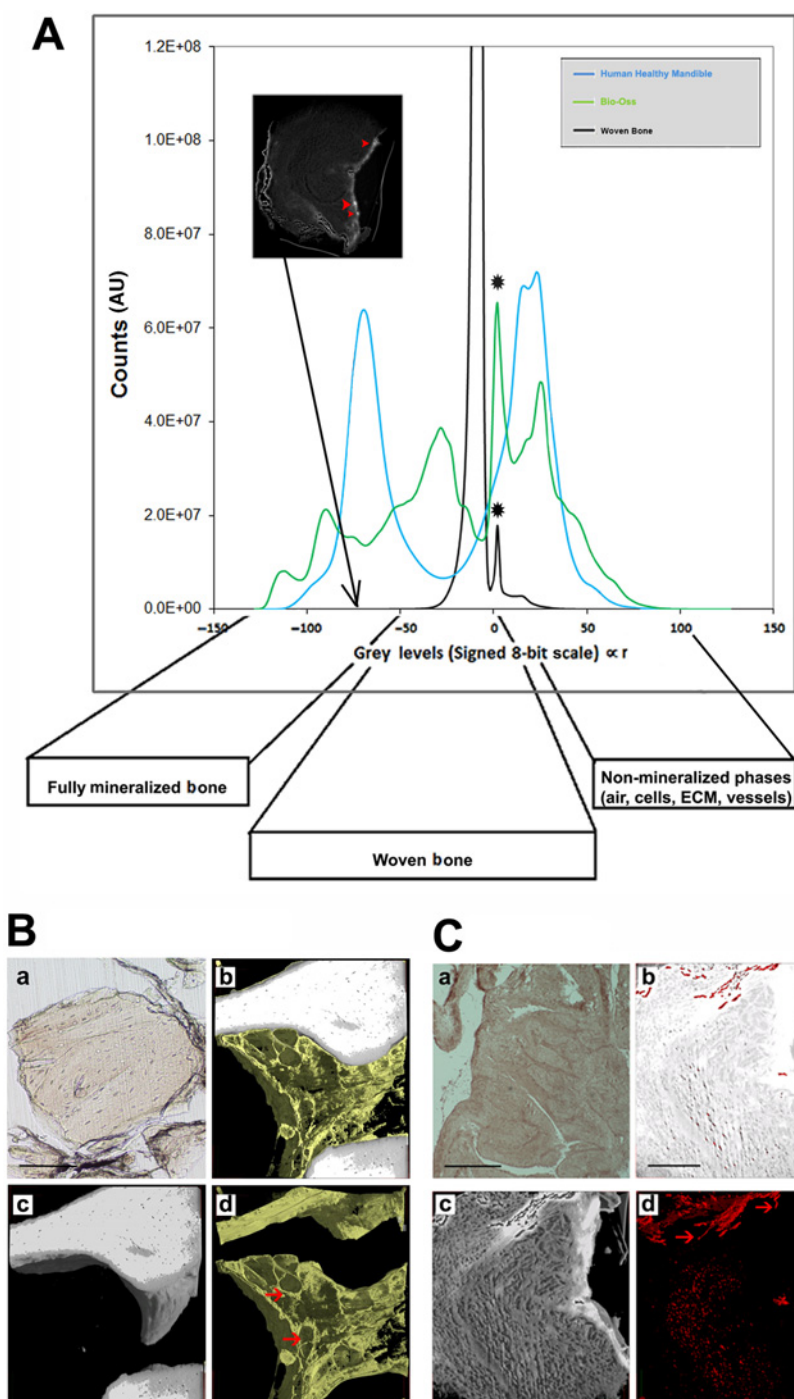
Figure 8. Histograms and 3D images of WB, Bio-Oss control and a human mandibular healthy site

(**A**) Grey-value distribution histograms of the samples obtained from WB, Bio-Oss control and a human mandibular healthy site. Peaks indicated with * are faked and due to mismatches of the samples in the field of view. (Top inset): 2D HT slice indicating few clusters of fully mineralized bone. (**B**) Three-dimensional images of Bio-Oss: (panel a) histological section with H&E staining, as a reference; (panels b–d) subvolume of the 3D HT reconstruction. To improve visualization, in each 3D image all phases were virtually deleted, except for: (b) bone and ECM, (c) bone and (d) ECM. Scale bar = 250 μm. (**C**) Three-dimensional images of WB sample: (a) histological section with H&E staining; (panels b–d) subvolume of the 3D HT reconstruction. To improve visualization, in each 3D image all phases were virtually deleted, except for: (b) woven bone and vessels, (c) WB and (d) vessels. Red arrowheads indicate portions of vessels to distinguish them from possible artefacts. Scale bar = 250 μm.

Bone ALP, a mature and late marker for osteoblastic differentiation, remained unchanged at 14 and 21 days, whereas it peaked at 7 days. RUNX2 and Osterix, the key transcription factors initiating and regulating early osteogenesis and late mineralization of bone, respectively [25,26], were found to be up-regulated. These data lead to the belief that a rather early osteogenic differentiation of DPSCs occurs. In previous studies [27] other researchers suggested that hDPSCs, cultured using HS, could be considered for cell therapy after a shorter period of expansion *in vitro*, but they did not obtain any bone sample in their experiments.

Another important issue to be considered is the vascular supply. In fact, when a tissue or organ is damaged, vascularization strongly contributes to the success of wound repair. Angiogenesis, as well as chemotaxis, homing and engraftment, are equally crucial to allow for the repair of an injured tissue by stem cells. Chemotactic stimuli recruit various cell types to the injury site. The interaction between the chemokine SDF1 and its receptor CXCR4, expressed on the hDPSC surface, is a key factor in the recruitment of these cells to the damaged area [28,29]. The increase in CXCR4 expression on hDPSCs, found in the present study, may also be of interest.

During tissue reparation, the migration and organization of endothelial cells into capillary tubes are regulated by a paracrine and autocrine action of VEGF [30]. When the damaged tissue involves bone, the cells located in its inner part have a limited blood and oxygen supply. This major issue must necessarily be overcome in order to obtain good results in clinical practice. To this end, we observed the expression of VEGF and PDGF-A. These significant findings led us to believe that angiogenesis in this setting is strongly enhanced. The presence of VEGF and PDGF-A in the microenvironment could also modulate the expression of their receptors in surrounding mesenchymal cells [31,32].

A very interesting feature of hDPSCs is their capability to fabricate WB tissue *in vitro*, which, after *in vivo* transplantation, is remodelled to highly vascularized bone tissue, with its main characteristics being deeply studied and understood in the present study using sophisticated analyses, including synchrotron-based phc-microCT and HT. We have assessed, using phc-microCT, that these WB samples are mainly constituted of WB tissue, with small clusters of mineralized bone that we have visualized and quantified. HT added fundamental information related to the mineralization level of the WB sample, strictly proportional to the physical mass density, ρ (expressed in mg/cm^3). It is interesting that the WB sample, even if mainly constituted of WB with lower mass density with respect to mandibular bone under remodelling and strongly lower mass density with respect to the deproteinized bone of bovine origin (Bio-Oss), presented few spots of fully mineralized bone formed after 40 days of culture. This finding is in agreement with phc-microCT data, suggesting more extensive growth after WB *in vivo* grafting.

Furthermore, HT showed, in 3D, new vessels in the WB samples, confirming deductions derived from the evidence that hDPSCs strongly expressed high levels of VEGF and PDGF-A. Therefore, the elevated expression of VEGF and PDGF-A correlates with vessel formation in the WB; this is of paramount interest for the physiology of the bone produced in order to also supply neoangiogenesis. All the previous data were confirmed after *in vivo* grafting, demonstrating that the WB samples, when transplanted into the subcutaneous sockets, show a periosteum and osteocytes that are clearly visible, and positive for OC and COLIA1 and that, above all, when grafted into a vertical mandibular bone defect, undergo, in addition to complete remodelling, integration with the surrounding bone, forming lamellar bone tissue in which haversian canals and osteocytes are clearly visible. It is of interest that, being produced by the stem cells from the participant who is undergoing grafting using a GMP-approved HS with no need for a scaffold, WB is an ideal new natural tool for bone tissue engineering, with the added value of being ready for transplantation without the need for scaffolds and cells, which often compromise the accomplishment of grafting.

Taken together, our results strongly indicate that hDPSCs exert exceptional differentiation capabilities towards osteoangiogenesis, representing the gold standard for obtaining well-vascularized bone. Moreover, DPSCs can give rise to bone tissue samples, represented by a vascularized WB, with histological and physical features, as confirmed by phc-microCT and HT analyses, that lead to the conclusion that WB is a very interesting customized tool, ready for regeneration.

Clinical perspectives

- Being human dental pulp stem cells (hDPSCs) able to differentiate in bone like tissues, this study aimed to establish if hDPSCs can lead to a bone tissue ready to be grafted for clinical application.

- The results showed that hDPSCs proliferate, differentiate into osteoblasts and express angiogenic genes such as VEGF and PDGFA. After 40 days of culture, hDPSCs, formed fibrous bone samples as demonstrated by Synchrotron-based X-ray phase-contrast microtomography, holotomography and histology. In addition, when transplanted in rats, WB samples formed a vascularized bone tissue.

- The data lead to the assumption that bone samples, fabricated by DPSCs, constitute a noteworthy tool do not requiring the use of scaffolds, therefore being ready for custom regeneration in bone regeneration.

Author contribution

M. La Noce, A. Giulani, V. Desiderio, S. Mazzonin and E. Amler collected and analysed the data. A. De Rosa and L. Laino selected patients and provided study material. G. Papaccio, V. Tirino and F. Paino conceived and designed the study, assembled the data and gave final approval for the manuscript. V. Tirino interpreted the data and wrote the manuscript.

Competing interest

The Authors declare that there are no competing interests associated with the manuscript.

Abbreviations

bALP, bone alkaline phosphatase; BSP, bone sialo-protein; COLIA1, type I collagen; CXCR4, chemokine receptor type 4; DMEM, Dulbecco's modified Eagle's medium; DSPP, dentin sialophosphoprotein; ECM, extracellular matrix; FBP, filtered-back projection; GAPDH, glyceraldehyde 3-phosphate dehydrogenase; GMP, good manufacturing practice; H&E, haematoxylin and eosin; hDPSC, human dental pulp stem cell; HS, human serum; HT, holotomography; ITGβ_1, integrin β_1; PDGF-A, platelet-derived growth factor A; phc-microCT, phase-contrast microtomography; OC, osteocalcin; OPN, osteopontin; TIE, transport of intensity equation; VEGF, vascular endothelial growth factor; WB, woven bone.

References

1 Caplan, A.I. (2007) Adult mesenchymal stem cells for tissue engineering versus regenerative medicine. J. Cell. Physiol. **213**, 341–347 CrossRef

2 Ferro, F., Spelat, R., Beltrami, A.P., Cesselli, D. and Curcio, F. (2012) Isolation and characterization of human dental pulp derived stem cells by using media containing low human serum percentage as clinical grade substitutes for bovine serum. PLoS One **7**, e48945 CrossRef

3 Laino, G., d'Aquino, R., Graziano, A., Lanza, V., Carinci, F., Naro, F. et al. (2005) A new population of human adult dental pulp stem cells: a useful source of living autologous fibrous bone tissue (LAB). J. Bone Miner. Res. **20**, 1394–1402 CrossRef

4 d'Aquino, R., Graziano, A., Sampaolesi, M., Laino, G., Pirozzi, G., De Rosa, A. et al. (2007) Human postnatal dental pulp cells codifferentiate into osteoblasts and endotheliocytes: a pivotal synergy leading to adult bone tissue formation. Cell Death Differ **14**, 1162–1171 CrossRef

5 Lizier, N.F., Kerkis, A., Gomes, C.M., Hebling, J., Oliveira, C.F., Caplan, A.I. et al. (2012) Scaling-up of dental pulp stem cells isolated from multiple niches. PLoS ONE **7**, e39885 CrossRef

6 Ponnaiyan, D., Bhat, K.M. and Bhat, G.S. (2012) Comparison of immuno-phenotypes of stem cells from human dental pulp and periodontal ligament. Int. J. Immunopathol. Pharmacol. **25**, 127–134 CrossRef

7 Paino, F., Ricci, G., De Rosa, A., d'Aquino, R., Laino, L., Pirozzi, G. et al. (2010) Ecto-mesenchymal stem cells from dental pulp are committed to differentiate into active melanocytes. Eur. Cell Mater. **20**, 295–305 CrossRef

8 Zhang, W., Walboomers, X.F., Shi, S., Fan, M. and Jansen, J.A. (2006) Multilineage differentiation potential of stem cells derived from human dental pulp after cryopreservation. Tissue Eng **12**, 2813–2823 CrossRef

9 Almushayt, A., Narayanan, K., Zaki, A.E. and George, A. (2006) Dentin matrix protein 1 induces cytodifferentiation of dental pulp stem cells into odontoblasts. Gene Therapy **13**, 611–620 CrossRef

10 Arthur, A., Rychkov, G., Shi, S., Koblar, S.A. and Gronthos, S. (2008) Adult human dental pulp stem cells differentiate toward functionally active neurons under appropriate environmental cues. Stem Cells **26**, 1787–1795 CrossRef

11 Lei, M., Li, K., Li, B., Gao, L.N., Chen, F.M. and Jin, Y. (2014) Mesenchymal stem cell characteristics of dental pulp and periodontal ligament stem cells after in vivo transplantation. Biomaterials **35**, 6332–6343 CrossRef

12 Paino, F., La Noce, M., Tirino, V., Naddeo, P., Desiderio, V., Pirozzi, G. et al. (2014) Histone deacetylase inhibition with valproic acid downregulates osteocalcin gene expression in human dental pulp stem cells and osteoblasts: evidence for HDAC2 involvement. Stem Cells **32**, 279–289 CrossRef

13 d'Aquino, R., De Rosa, A., Lanza, V., Tirino, V., Laino, L., Graziano, A. et al. (2009) Human mandible bone defect repair by the grafting of dental pulp stem/progenitor cells and collagen sponge biocomplexes. Eur. Cell Mater. **18**, 75–83 CrossRef

14 Giuliani, A., Manescu, A., Langer, M., Rustichelli, F., Desiderio, V., Paino, F. et al. (2013) Three years after transplants in human mandibles, histological and in-line holotomography revealed that stem cells regenerated a compact rather than a spongy bone: biological and clinical implications. Stem Cells Transl. Med. **2**, 316–324 CrossRef

15 Tatullo, M., Marrelli, M., Shakesheff, K.M. and White, L.J. (2015) Dental pulp stem cells: function, isolation and applications in regenerative medicine. J. Tissue Eng. Regen. Med. **9**, 1205–1216 CrossRef

16 Albertini, G., Giuliani, A., Komlev, V., Moroncini, F., Pugnaloni, A., Pennesi, G. et al. (2009) Organization of extracellular matrix fibers within polyglycolic acid-polylactic acid scaffolds analyzed using X-ray synchrotron-radiation phase-contrast micro computed tomography. Tissue Eng. Part C Methods **15**, 403–411 CrossRef

17 Giuliani, A., Moroncini, F., Mazzoni, S., Belicchi, M.L., Villa, C., Erratico, S. et al. (2014) Polyglycolic acid-polylactic acid scaffold response to different progenitor cell in vitro cultures: a demonstrative and comparative X-ray synchrotron radiation phase-contrast microtomography study. Tissue Eng. Part C Methods **20**, 308–316 CrossRef

18 Sidell, D.R., Aghaloo, T., Tetradis, S., Lee, M., Bezouglaia, O., DeConde, A. et al. (2012) Composite mandibulectomy: a novel animal model. Otolaryngol. Head Neck Surg. **146**, 932–937 CrossRef

19 Fan, J., Park, H., Lee, M.K., Bezouglaia, O., Fartash, A., Kim, J. et al. (2014) Adipose-derived stem cells and BMP-2 delivery in chitosan-based 3D constructs to enhance bone regeneration in a rat mandibular defect model. Tissue Eng. Part A **20**, 2169–2179 CrossRef

20 Wu, X. and Yan, A. (2009) Phase retrieval from one single phase contrast x-ray image. Opt. Express **17**, 11187–11196 CrossRef

21 Arfelli, F., Assante, M., Bonvicini, V., Bravin, A., Cantatore, G., Castelli, E. et al. (1998) Low-dose phase contrast X-ray medical imaging. Phys. Med. Biol. **43**, 2845–2852 CrossRef

22 Hofmann, R., Moosmann, J. and Baumbach, T. (2011) Criticality in single-distance phase retrieval. Opt. Express **19**, 25881–25890 CrossRef

23 Langer, M., Cloetens, P. and Peyrin, F. (2010) Regularization of phase retrieval with phase-attenuation duality prior for 3D holotomography. IEEE Trans. Image Process **19**, 2428–2436 CrossRef

24 Neve, A., Corrado, A. and Cantatore, F.P. (2013) Osteocalcin: skeletal and extra-skeletal effects. J. Cell Physiol. **228**, 1149–1153 CrossRef

25 Zhou, X., Zhang, Z., Feng, J.Q., Dusevich, V.M., Sinha, K., Zhang, H. et al. (2010) Multiple functions of Osterix are required for bonegrowth and homeostasis in postnatal mice. Proc. Natl. Acad. Sci. U.S.A. **107**, 12919–12924 CrossRef

26 Bruderer, M., Richards, R.G., Alini, M. and Stoddart, M.J. (2014) Role and regulation of RUNX2 in osteogenesis. Eur. Cell Mater. **28**, 269–286 CrossRef

27 Pisciotta, A., Riccio, M., Carnevale, G., Beretti, F., Gibellini, L., Maraldi, T. et al. (2012) Human serum promotes osteogenic differentiation of human dental pulp stem cells in vitro and in vivo. PLoS One **7**, e50542 CrossRef

28 Jiang, L., Zhu, Y.Q., Du, R., Gu, Y.X., Xia, L., Qin, F. et al. (2008) The expression and role of stromal cell-derived factor-1alpha–CXCR4 axis in human dental pulp. J. Endod. **34**, 939–944 CrossRef

29 Kim, D.S., Kim, Y.S., Bae, W.J., Lee, H.J., Chang, S.W., Kim, W.S. et al. (2013) The role of SDF-1 and CXCR4 on odontoblastic differentiation in human dental pulp cells. Int. Endod. J. **47**, 534–541 CrossRef

30 Lamalice, L., Le Boeuf, F. and Huot, J. (2007) Endothelial cell migration during angiogenesis. Circ. Res. **100**, 782–794 CrossRef

31 Ball, S.G., Shuttleworth, C.A. and Kielty, C.M. (2007) Mesenchymal stem cells and neovascularization: role of platelet-derived growth factor receptors. J. Cell. Mol. Med. **11**, 1012–1030 CrossRef

32 Brudno, Y., Ennett-Shepard, A.B., Chen, R.R., Aizenberg, M. and Mooney, D.J. (2013) Enhancing microvascular formation and vessel maturation through temporal control over multiple pro-angiogenic and pro-maturation factors. Biomaterials **34**, 9201–9209 CrossRef